Soft X-ray Photoemission Study of Thermoelectric Alloys $Fe_{2-x-y}Ir_yV_{1+x}Al$ and $Fe_{2-x}V_{1+x-y}Ti_yAl$

Kazuo Soda[a,*], Shota Harada[a], Masahiko Kato[a], Shinya Yagi[a],
Manabu Inukai[b], Hidetoshi Miyazaki[c],
Yusuke Sandaiji[d], Yuko Tamada[d], Suguru Tanaka[d], Takahiro Sugiura[d], Yoichi Nishino[d]

[a]Department of Quantum Engineering, Graduate School of Engineering, Nagoya University, Furo-cho, Chikusa-ku, Nagoya 464-8603, Japan
[b]Japan Synchrotron Radiation Research Institute, 1-1-1 Kouto, Sayo-cho, Sayo-gun 679-5198, Japan
[c]Institute for Molecular Science, Myodaiji-cho, Okazaki 444-8585, Japan
[d]Department of Frontier Materials, Graduate School of Engineering, Nagoya Institute of Technology, Gokiso-cho, Showa-ku, Nagoya 466-8555, Japan

The valence-band and core-level photoemission spectra of n-type thermoelectric Heusler($L2_1$)-type alloys $Fe_{2-x-y}Ir_yV_{1+x}Al$ and p-type ones $Fe_{2-x}V_{1+x-y}Ti_yAl$ have been studied to clarify the origin of the enhancement of their thermoelectric power. It is found that the excess V content x (V-rich for $x > 0$ and Fe-rich for $x < 0$) causes the drastic change in the valence-band electronic structure within the binding energy of ~0.7 eV near the Fermi level E_F and the evolution of the satellite structures in the V 2*p* core-level spectra with x increased. These spectral features are ascribed to the formation of the Fe or V anti-site defects in the off-stoichiometric alloys with non-zero x. The shift of the valence-band and core-levels towards the high (low) binding energy side is observed on partial substitution y of Ir (or Ti) for Fe (or V), which is attributed to the E_F shift due to the common band formation with the Ir 5*d* or Ti 3*d* states incorporated into the main Fe-V 3*d* bands. The enhancement of the thermoelectric power in those Heusler-type alloys can be explained in terms of the observed changes in the valence-band electronic structure near E_F.

Keywords: X-ray photoelectron spectroscopy, Electronic structure, Thermoelectric power, Anti-site defects, $Fe_{2-x-y}Ir_yV_{1+x}Al$, $Fe_{2-x}V_{1+x-y}Ti_yAl$

*Corresponding author at: Department of Quantum Engineering, Graduate School of Engineering, Nagoya University, Furo-cho, Chikusa-ku, Nagoya 464-8603, Japan.
E-mail address: j45880a@nucc.cc.nagoya-u.ac.jp

1. Introduction

Heusler($L2_1$)-type Fe_2VAl-based alloys have received much attention because of their potential application for thermoelectric materials [1]. They are superior to commercially available thermoelectric materials such as Bi-(Te,Sb) semiconductors in costs, environmental load and mechanical strengths; they have been tentatively applied for a thermoelectric power generator on motorcycles [2]. Theoretical studies [3, 4] predicted a semi-metallic electronic band structure with a sharp pseudogap just at the Fermi energy E_F for stoichiometric Fe_2VAl, which was experimentally confirmed by infra-red spectroscopy [5] and soft X-ray photoemission spectroscopy (XPS) [6]. According to the Boltzmann transport equation, this electronic band structure may lead to the enhancement of their thermoelectric power on partial substitution of the constituent elements by the forth one or on off-stoichiometric concentration change, since the thermoelectric power $S(T)$ at temperature T may be given by the first-order energy moment of the electronic density of states (DOS) $N(E)$ around the chemical potential $\mu \sim E_F$ in the energy range between $\mu - 2k_BT$ and $\mu + 2k_BT$ [7]:

$$S(T) \cong \frac{1}{eT} \frac{\int N(E)(E-\mu)\frac{\partial f(E;T)}{\partial E} dE}{\int N(E)\frac{\partial f(E;T)}{\partial E} dE} \quad . \qquad (1)$$

Here, $f(E;T)$ is the Fermi-Dirac distribution function and its energy derivative works as an energy window of $\sim 2k_BT$ in width. In fact, a universal dependence of thermoelectric power on substitution has been observed [1]; as shown in Fig.1, experimental thermoelectric powers at T = 300 K of several types of partially substituted alloys such as $Fe_{2-y}Re_yVAl$, $Fe_2V_{1-y}Ti_yAl$ and $Fe_2VAl_{1-z}Si_z$ [8-11] are around a grey curve, which represents thermoelectric powers estimated from eq. (1) with a theoretical DOS of Fe_2VAl [3, 7], by plotting them as a function of averaged valence electron counts per constituent atom (hereafter referred to as VEC). However, thermoelectric powers of off-stoichiometric alloys $Fe_{2-x}V_{1+x}Al$ show a qualitatively quite different behavior, as shown by open circles in Fig. 1. Further enhancement of thermoelectric powers has been found for alloys with both the off-stoichiometric concentration change (off-stoichiometric V/Fe ratio with excess V content x) and partial substitution y: the n-type $Fe_{2-x-y}Ir_yV_{1+x}Al$ [12] and p-type $Fe_{2-x}V_{1+x-y}Ti_yAl$ [13] (closed circles in the figure for y = 0.03). These findings suggest that the off-stoichiometric V/Fe ratio may cause a drastic change in the electronic structure near E_F, which has been discussed by theoretical calculations [4, 14, 15, 16] in relation with a heavy-Fermion-like properties of Fe_2VAl at low temperatures [17].

In this paper, we will report the results of the soft x-ray photoemission study of $Fe_{2-x-y}Ir_yV_{1+x}Al$ and $Fe_{2-x}V_{1+x-y}Ti_yAl$ for understanding the origin of the further enhancement of their thermoelectric powers. We have observed the systematic change in the valence-band and core-level spectra by bulk-sensitive high-resolution XPS and will discuss the change in the electronic structure induced by the partial substitution and off-stoichiometry of the V/Fe ratio. A part of the results on $Fe_{2-x-y}Ir_yV_{1+x}Al$ has been already reported elsewhere [18].

2. Experimental

Polycrystalline specimens of 1 x 1 x 3 mm^3 in typical size were prepared by arc-melting of mixture of appropriate composition of Fe, V and Al, subsequent annealing to obtain the homogenized and ordered $L2_1$ structure, shaping and re-annealing, as described in detail elsewhere [3, 12, 13, 19]. Clean surfaces for photoelectron measurement were obtained by *in situ* fracturing the specimens at low temperatures with a knife edge. This procedure reduces the effects due to surface deterioration [20, 21], and the surface components were estimated to be less than 0.2 from the V 2*p* spectrum as in the previous reports [21, 22, 23]. There were no signals other than the constituent elements recognized in the wide ranging XPS spectra measured just after fracturing, and no O 1*s* signals were noticed to appear during the present measurement.

Photoemission measurements were performed at BL27SU of SPring-8, Japan Synchrotron Radiation Research Institute (JASRI). Photoelectron spectra were recorded at 10 K in the angle-integrated mode with a hemispherical analyzer (PHOIBOS 150) and linearly polarized excitation photons from an undulator [24]. Total energy resolution and the origin of the binding energy, E_B, *i.e.* the Fermi energy E_F, were determined by measuring the Fermi edge of evaporated Au films. The energy resolution was estimated to be 0.16 eV at the excitation photon energy $h\nu$ of ~1000 eV. The drift of the excitation photon energy was also calibrated by frequently measuring the Au $4f_{7/2}$ core-level spectrum during the measurement of the specimens, and the error in the energy position of E_F is estimated to be less than 0.02 eV. This calibration procedure enables us to investigate the change in the valence-band structure near E_F in spite of the semimetallic nature of studied alloys. Although the energy resolution is not so sufficient to directly clarify the electronic structure within ~0.05 eV around E_F, which is related to the thermoelectric power at T = 300 K, the spectral features near E_F shed light on the thermoelectric properties, as shown later.

3. Results and discussion

Figure 2 shows typical valence-band spectra near E_F of $Fe_{2-x}V_{1+x}Al$, comparing them with several calculated DOS [4, 7, 15, 16]. The intensities of these spectra are normalized with the integrated intensity up to E_B = 3.8 eV, which may correspond to the main 3*d* band. As already reported [7, 13, 18, 23], the valence-band spectrum does not so much alter as a whole with *x*, except for small overall shift, which is expected from the change in VEC and hence E_F, and emergence of new features between E_F and E_B ~0.7 eV.

For the stoichiometric Fe_2VAl, the valence-band spectrum agrees fairly well with a total DOS calculated by an all-electron full-potential linearized augmented plane wave (FLAPW) method with WIEN2k code [25] using the experimental lattice constant a = 0.5761 nm [17]. As seen in the figure, occupied states (“valence” band) near E_F and a band around E_B ~ 0.8 eV mainly consist of the Fe 3*d* states and a band at E_B ~ 1.6 eV is composed of hybridized Fe and

V 3*d* states, while the lowest unoccupied states ("conduction" band) near E_F comprises the V 3*d* states [3, 4, 16]. Although it is unable to investigate the unoccupied DOS by normal photoelectron spectroscopy, intensity decrease towards E_F and a weak shoulder structure near E_F indicate the existence of the predicted pseudogap. Observed large intensity around E_F, compared to the calculated DOS, may be partly due to the surface component, which less contributes to the valence-band spectrum than the V 2*p* one because of the larger kinetic energy of photoelectrons from the valence-band. It is also partly attributed to the anti-site defect states in this specimen [19], as discussed later. Other possible reasons are based on the apparent ~0.2-eV shift of the observed spectra to the low binding energy in comparison with the calculated DOS: narrowing of the pseudogap than theoretically expected and pinning of E_F at the low energy side of the pseudogap. According to a study of Heusler-type alloys $(Fe_{2/3}V_{1/3})_{100-y}Al_y$ [6], the small positive thermoelectric power (~30 μVK^{-1} at 300 K) of Fe_2VAl is attributed to less contribution of the unoccupied DOS just above E_F than the occupied one just below E_F, as predicted by band structure calculation (see the gray curve in Fig.1 [6, 7]). This is also supported by observed positive Hall coefficient $R_H \sim 2 \times 10^{-8}$ m^3C^{-1} at 300 K [11].

For the off-stoichiometric V/Fe ratio, the spectral shape, in particular below $E_B \sim 0.7$ eV, is much altered in spite of small change in the excess V content *x*: $Fe_{2.04}V_{0.96}Al$ shows a steep rise just below E_F and an increasing new band at $E_B \sim 0.3$ eV, while $Fe_{1.98}V_{1.02}Al$ still reveals a clear shoulder structure near E_F and an increased intensity at $E_B \sim 0.5$ eV. These drastic changes near E_F are caused by excess Fe and V atoms occupying normal V and Fe sites in the $L2_1$ structure, respectively, *i.e.* anti-site Fe and V defects, because their symmetry and chemical environment are quite different from those at their normal site.

Focusing on change in the local electronic states induced by the concentration change, particularly such anti-site defects, we have investigated the 2*p* core-levels of Fe, V, and Al. As already reported for $Fe_{2-x-y}Ir_yV_{1+x}Al$ [18], we have found additional chemically-shifted satellite structures increasing with *x* for the V 2*p* core-level spectra but not for the Fe and Al 2*p* spectra. According to the previous studies [18, 22, 23], the satellite structure is composed mainly of the chemically shifted components of the anti-site V, V neighboring at the substituted element, and V in the surface layer. Similarly, the satellite structures of $Fe_{2-x}V_{1+x}Al$ include contributions from both the anti-site and surface V. Although no clearly peaked structures are observed, satellite structures are recognized in the low binding energy side of the main lines. This suggests the increase in the local VEC at the anti-site V.

Changes in the local VEC and the local electronic structure around the anti-site defects are related to the electronic structures of Fe_3Al and Fe_2VAl and their site-selectivity for the substituted forth element [3, 4, 26]. According to band structure calculations [4, 26], Fe at the Fe(II) site in $D0_3$-type Fe_3Al (the Fe site in $L2_1$-type Fe_2VAl) possesses relatively increased valence electrons and is negatively charged in comparison with Fe at the Fe(I) site (the V site in Fe_2VAl). This suggests that an element with less valence electrons than Fe, such as V and

Ti, may tend to occupy the Fe(I) site, whereas an element with more valence electrons such as Ir may favor the Fe(II) site, because of increasing Coulomb energy [4]. In turn, the anti-site V, *i.e.* V at the Fe(II) site, is expected to have more valence electrons than V at the Fe(I) site (the normal V site of Fe_2VAl), which is observed as the chemically shifted component in the present V 2*p* spectrum.

On the other hand, Fe_2VAl has the electron pockets at the X point, consisting of the V 3*d* states, and the hole pocket at the Γ point, mainly composed of the Fe 3*d* states [3, 4]. Although the unoccupied states cannot be clarified by the present photoelectron spectroscopy, the anti-site V may induce a new state, probably an anti-bonding state with nearest neighboring V around the anti-site V, in the unoccupied part of the pseudogap; a bonding state may correspond to the increasing band observed at $E_B \sim 0.5$ eV for $x > 0$. The anti-site Fe, Fe at the Fe(I) site, with less valence electrons may form a body-centered cubic Fe-like local structure, leading to the increasing band at $E_B \sim 0.3$ eV in the occupied part of the pseudogap for $x < 0$.

In Fig.2, we compare the spectra with total DOS (thick solid curves), calculated by a linear muffin-tin orbital atomic sphere approximation (LMTO-ASA) method with a supercell of x = -0.125 and +0.125 for ferromagnetic states [15], local partial DOS (broken curves) of the anti-site Fe for $x = 0$ (as-Fe) [4], which was calculated for Fe_2GaAl but is here presented because of their argument of close similarity between Fe_2VAl and Fe_2GaAl, and local partial DOS of the anti-site V for x = +0.06 (as-V) [16]. The local partial DOS of the anti-site Fe and V are calculated by a Korringa-Kohn-Rostoker method with a coherent-potential approximation (KKR-CPA). According to these theoretical studies, the majority- and minority-spin states of V appear ~0.2 eV below and above E_F for $x > 0$ (V-rich); in KKR-CPA, these spin states of the anti-site V, split by ~0.3 eV, form an apparent single peak at E_F. For $x < 0$ (Fe-rich), the majority-spin states of the anti-site Fe appear around $E_B \sim 0.5$ eV in both calculations and another weak band around E_F in LMTO-ASA.

Comparison between these calculated DOS and the observed spectra suggests that the newly emerging band at $E_B \sim 0.3$ eV may correspond to the majority-spin states of the anti-site Fe predicted at $E_B \sim 0.5$ eV. However, the anti-site V states are difficult to assign in the observed spectrum; the above-mentioned apparent shift might push the anti-site V states above E_F. If this is the case, the observed sign of the thermoelectric power of $Fe_{2-x}V_{1+x}Al$, positive for $x < 0$ (Fe-rich) and negative for $x > 0$ (V-rich), can be qualitatively explained through eq. (1) with the anti-site defect states below and above E_F, respectively. This is also consistent with the results of the Hall coefficient measurement of our polycrystalline samples.

To study the effect of the partial substitution, we compare the spectra of substituted alloys $Fe_{1.97-x}Ir_{0.03}V_{1+x}Al$ and $Fe_{2-x}V_{0.97+x}Ti_{0.03}Al$ with those of $Fe_{1-x}V_{1+x}Al$ at fixed x in Fig. 3. As seen in the figure, the Ir substitution causes very small but rigid shift of the leading edge of the first *d*-band with a shoulder structure towards the high binding energy side and reduces the intensity within ~0.1 eV near E_F, which may enhance the negative thermoelectric power. For

Ti substitution, the first *d*-band shows 0.05~0.1-eV shift towards the low binding energy side, although the relative intensity of the shoulder structure at E_B ~ 0.3 eV is increased. Disappearance of the shoulder structure near E_F seems to agree with the decrease of VEC induced by Ti substitution. It is also found that the V 2*p* main line is shifted by ~0.1 eV towards the low binding energy side on Ti substitution, while it shows small shift to the high binding energy side on Ir substitution. Thus, the partial substitution *y* of Ir and Ti is more or less in qualitative accordance with a rigid band model, where the increase (decrease) of VEC induced by the atomic concentration change would shift the position of E_F towards the low (high) binding energy side without the electronic structure altered, and hence observed spectra would simply move towards the high (low) binding energy side. This moderate shift on the partial substitution can be explained by the common band formation [4, 27] with the *d* states of the substituted elements in the neighboring column of the periodic table (Ir and Ti in the present case) incorporated into the main Fe-V 3*d* valence-bands. Since the *d* states of the neighboring elements are energetically close to the Fe or V 3*d* states, they would not affect the main Fe-V 3*d* band near E_F so much by the common band formation.

Although the unoccupied states above E_F cannot be observed by the present photoelectron spectroscopy, the emergence of the anti-site defect states near E_F as well as the shift of E_F by the partial substitution can explain the enhancement of the thermoelectric power in the n-type $Fe_{2-x-y}Ir_yV_{1+x}Al$ and p-type $Fe_{2-x}V_{1+x-y}Ti_yAl$, as follows. In $Fe_{2-x}V_{1+x}Al$, the increase in the DOS just below E_F by the anti-site Fe states at E_B ~ 0.3 eV for $x < 0$ results in the positive thermoelectric power as the “valence”-band top, while that in the V 3*d* DOS just above E_F without change in the shoulder structure near E_F for $x > 0$ leads to the negative thermoelectric power as the “conduction”-band bottom. Further substitution of Ir and Ti shifts E_F more or less in a rigid-band manner to increase respective DOS just above and below E_F, and it enhances the negative and positive thermoelectric power in $Fe_{2-x-y}Ir_yV_{1+x}Al$ and $Fe_{2-x}V_{1+x-y}Ti_yAl$, respectively.

4. Conclusions

The valence-band and core-level spectra have been investigated for the thermoelectric materials $Fe_{2-x-y}Ir_yV_{1+x}Al$ and $Fe_{2-x}V_{1+x-y}Ti_yAl$. The excess V for $x > 0$ (or excess Fe for $x < 0$) causes the drastic change in the valence-band electronic structure through the anti-site V (or Fe) defect formation, while the partial substitution *y* of Ir and Ti for Fe and V, respectively, induces the moderate shift of the whole valence-band, which is attributed to the common band formation with the Ir 5*d* or Ti 3*d* states incorporated into the main Fe-V 3*d* bands. The enhancement of thermoelectric power in these alloys can be explained qualitatively by the observed change in the electronic structure near E_F. The present study has demonstrated the importance of adjusting the electronic states by nano-structures such as the anti-site defect in the functional materials.

Acknowledgements

Soft x-ray photoelectron measurements were performed at the beamline BL27SU of SPring-8 under the Priority Nanotechnology Support Program administered by the Japan Synchrotron Radiation Research Institute (JASRI) (Proposal Nos. 2009A1672 and 2009B1729). We appreciate Dr. S. Fujii showing their detailed data of super-cell calculations for $Fe_{2-x}V_{1+x}Al$.

References

[1] Y. Nishino, in: T. B. Massalski and P. E. Turchi (Eds.), The Science of Complex Alloy Phases, TMS, Warrendale, 2005, pp. 325-344.

[2] Y. Nishino, M. Mikami, Kinzoku **79** (2009) 231-236.

[3] G. Y. Guo, G. A. Botton, Y. Nishino, J. Phys.: Condens. Matter **10** (1998) L119.

[4] A. Bansil, S. Kaprzyk, P. E. Mijnarends, J. Tobola, Phys. Rev. B **60** (1999) 13396-13412.

[5] H. Okamura, J. Kawahara, T. Namba, S. Kimura, K. Soda, U. Mizutani, Y. Nishino, M. Kato, I. Shimoyama, H. Miura, K. Fukui, K. Nakagawa, H. Nakagawa, T. Kinoshita, Phys. Rev. Lett. **84** (2000) 3674.

[6] K. Soda, H. Murayama, K. Shimba, S. Yagi, J. Yuhara, T. Takeuchi, U. Mizutani, H. Sumi, M. Kato, H. Kato, Y. Nishino, A. Sekiyama, S. Suga, T. Matsushita, Y. Saitoh, Phys. Rev. B **71** (2005) 245112.

[7] K. Soda, H. Miyazaki, K. Yamamoto, T. Mochizuki, M. Iukai, M. Kato, S. Yagi, Y. Nishino, Adv. Synchrotron Rad. **1** (2008) 235-243.

[8] F. Kobayashi, N. Ide, Y. Nishino, J. Japan Inst. Metals **71** (2007) 208-212.

[9] H. Matsuura, Y. Nishino, U. Mizutani, S. Asano, J. Japan. Inst. Metals **66** (2002) 767-771.

[10] H. Kato, M. Kato, Y. Nishino, U. Mizutani, S. Asano, J. Japan. Inst. Metals **65** (2001) 652-656.

[11] Y. Nishino, S. Deguchi, U. Mizutani, Phys. Rev. B**74** (2006) 115115-1-6.

[12] T. Sugiura, Y. Nishino, J. Japan Inst. Metals **73** (2009) 846-851.

[13] Y. Sandaiji, N. Ide, Y. Nishino, T. Owada, S. Harada, K. Soda, J. Jpn. Soc. Powder Powder Metallurgy **57** (2010) 207-212.

[14] J. Deniszczyk, Acta Phys. Pol. B **32** (2001) 529-533.

[15] S. Fujii, Y. Ienaga, S. Ishida, S. Asano, J. Phys. Soc. Jpn. **72** (2003) 698-704.

[16] V. N. Antonov, A. Ernst, I. V. Maznichenko, A. N. Yaresko, A. P. Shpak, Phys. Rev. B **77** (2008) 134444.

[17] Y. Nishino, M. Kato, S. Asano, K. Soda, M. Hayasaki, U. Mizutani, Phys. Rev. Lett. **79** (1997) 1909-1912.

[18] S. Harada, T. Ohwada, M. Inukai, M. Kato, S. Yagi, K. Soda, H. Miyazaki, Y. Sandaiji, T. Sugiura, Y. Nishino, J. Jpn. Soc. Powder Powder Metallurgy **57** (2010) 213-217.

[19] Y. Nishino, H. Sumi, U. Mizutani, Phys. Rev. B **71** (2005) 094425.

[20] K. Soda, T. Mizutani, O. Yoshimoto, S. Yagi, U. Mizutani, H. Sumi, Y. Nishino, Y.

Yamada, T. Yokoya, S. Shin, A. Sekiyama, S. Suga, J. Synchrotron Rad. **9** (2002) 223-236.
[21] K. Soda, H. Murayama, S. Yagi, M. Kato, T. Takeuchi, U. Mizutani, S. Imada, S. Suga, Y. Saitoh, T. Muro, H. Sumi, Y. Nishino, Physica. B **351** (2004) 338-340.
[22] H. Miyazaki, K. Soda, S. Yagi, M. Kato T. Takeuchi, U. Mizutani, Y. Nishino, J. Vac. Sci. Technol. A**24** (2006) 1464-1467.
[23] H. Miyazaki, K. Soda, M. Kato, S. Yagi, T. Takeuchi, Y. Nishino, J. Electron Spectrosc. Relat. Phenom. **156-158** (2007) 347-350.
[24] H. Ohashi, E. Ishiguro, H. Okumura, A. Hiraya, Y. Senba, K. Okada, N. Saito, I. Suzuki, K. Ueda, T. Ibuki, S. Nagaoka, I. Koyano, T. Ishikawa, Nucl. Instrum. Methods A **467** (2001) 533-536.
[25] K. Schwarz, P. Blaha, G. K. H. Madsen, Comp. Phys. Commun. **147** (2002) 71.
[26] S. Ishida, J. Ishida, S. Asano, J. Yamashita, J. Phys. Soc. Jpn. **41** (1976) 1570-1574.
[27] A. P. Sutton, Electronic Structure of Materials, Clarendon Press, Oxford, 1996, pp. 189-193.

Figure captions

Fig. 1. Thermoelectric powers at 300 K on various Heusler-type Fe_2VAl-based alloys. The abscissa is averaged valence electron counts per constituent atom. A grey curve (DOS) shows thermoelectric powers estimated from a theoretical density of states for Fe_2VAl within a rigid band picture. Figures besides symbols indicate the excess V content x in $Fe_{2-x}V_{1+x}Al$, $Fe_{1.97-x}Ir_{0.03}V_{1+x}Al$ and $Fe_{2-x}V_{0.97+x}Ti_{0.03}Al$.

Fig. 2. Valence-band photoelectron spectra near the Fermi level of $Fe_{2-x}V_{1+x}Al$. Theoretical densities of states are shown for comparison. For off-stoichiometric alloys (non-zero x), local partial densities of states of the anti-site Fe (as-Fe) or V (as-V) are also presented by broken curves.

Fig. 3. Valence-band photoelectron spectra near the Fermi level of $Fe_{2-x}V_{1+x}Al$, $Fe_{1.97-x}Ir_{0.03}V_{1+x}Al$ and $Fe_{2-x}V_{0.97+x}Ti_{0.03}Al$. The Fermi edge of a reference Au is also shown for comparison.

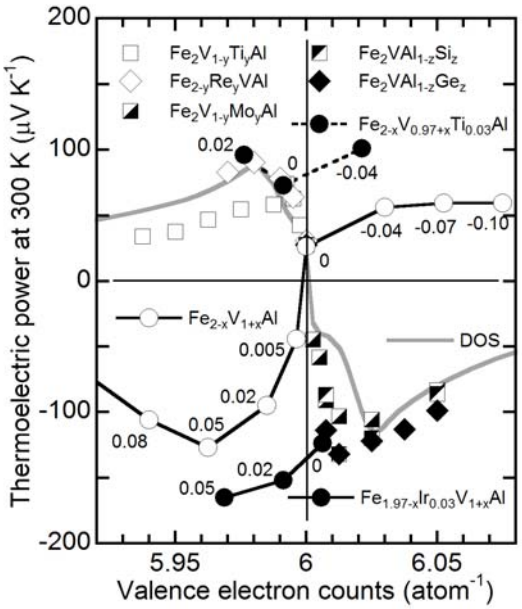
Thermoelectric power at 300 K (μV K-1)
Valence electron counts (atom-1)
Fe2V1-yTiyAl
Fe2-yReyVAl
Fe2V1-yMoyAl
Fe2VAl1-zSiz
Fe2VAl1-zGez
Fe2-xV0.97+xTi0.03Al
Fe2-xV1+xAl
Fe1.97-xIr0.03V1+xAl
DOS

Fig. 1

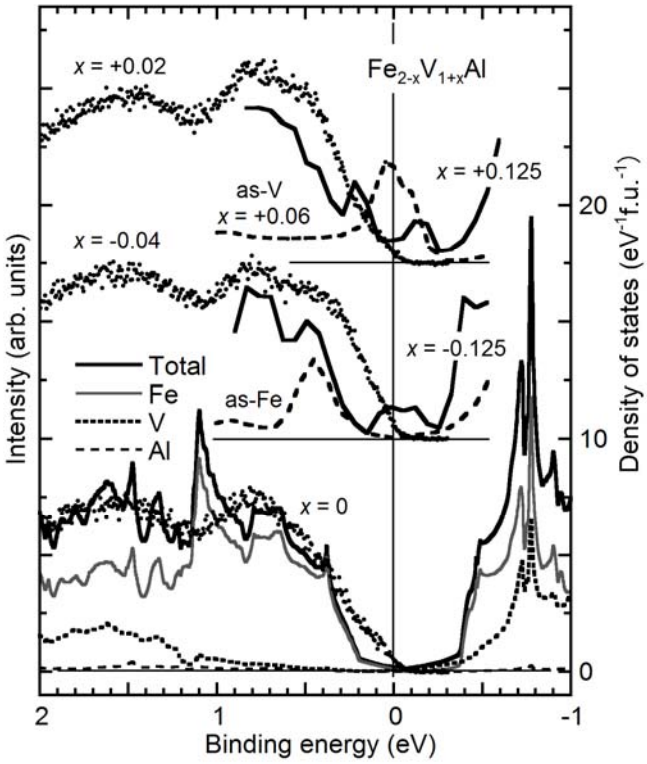
x = +0.02
Fe2-xV1+xAl
x = +0.125
as-V
x = +0.06
x = -0.04
x = -0.125
as-Fe
Total
Fe
V
Al
x = 0
Intensity (arb. units)
Density of states (eV-1f.u.-1)
Binding energy (eV)

Fig.2

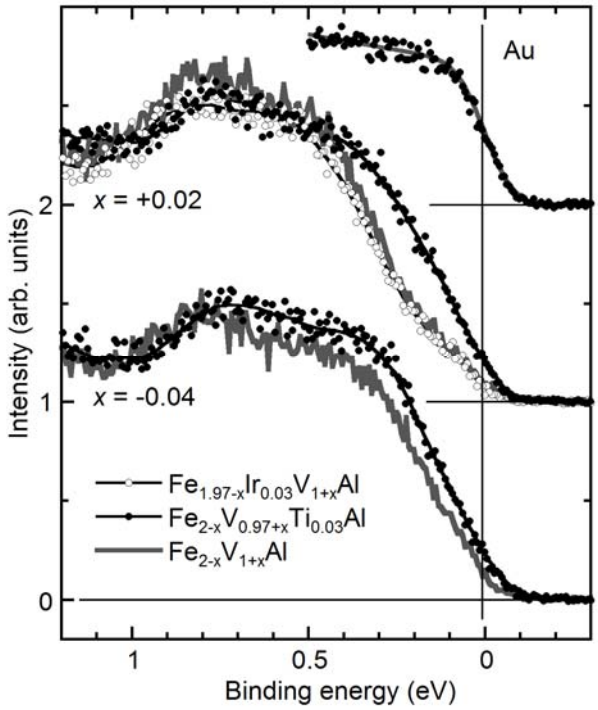
Au
x = +0.02
x = -0.04
Fe1.97-xIr0.03V1+xAl
Fe2-xV0.97+xTi0.03Al
Fe2-xV1+xAl
Intensity (arb. units)
Binding energy (eV)
2
1
0
1
0.5
0

Fig.3